Blood First Edition Paper, prepublished online July 16, 2018; DOI 10.1182/blood-2018-03-836601

Therapeutic vulnerability of multiple myeloma to MIR17PTi, a first-in-class inhibitor of pri-mir-17-92

Eugenio Morelli[1,2], Lavinia Biamonte[1], Cinzia Federico[1,3], Nicola Amodio[1], Maria Teresa Di Martino[1], Maria Eugenia Gallo Cantafio[1], Martina Manzoni[4,5], Francesca Scionti[1], Mehmet Kemal Samur[2], Annamaria Gullà[1,2], Maria Angelica Stamato[1], Maria Rita Pitari[1], Daniele Caracciolo[1], Settimio Sesti[6], Niels M. Frandsen[7], Marco Rossi[1], Antonino Neri[4,5], Mariateresa Fulciniti[2], Nikhil C. Munshi[2,8], Pierosandro Tagliaferri[1], and Pierfrancesco Tassone[1].

[1]Department of Experimental and Clinical Medicine, Magna Graecia University, Salvatore Venuta University Campus, Catanzaro, 88100, Italy.

[2]Jerome Lipper Multiple Myeloma Center, Department of Medical Oncology, Dana-Farber Cancer Institute, Boston, MA, 02215, USA.

[3]Department of Radiation Oncology, Cancer Biology division, Washington University in Saint Louis School of Medicine, Saint Louis, MO, USA.

[4]Department of Oncology and Oncoematology, University of Milan, Milan, Italy.

[5]UOC Ematologia, Fondazione Cà Granda IRCCS, Ospedale Maggiore Policlinico, Milan, Italy.

[6]Department of Biology, Ecology and Earth Science, University of Calabria, Cosenza, 87100, Italy.

[7]Exiqon A/S, Skelstedet 16, 2950 Vedbaek, Denmark.

[8]VA Boston Healthcare System, West Roxbury, Boston, MA, USA.

Corresponding author: Pierfrancesco Tassone, MD, Magna Graecia University, Viale Europa, 88100 Catanzaro, Italy; E-mail: tassone@unicz.it, Phone: +39-0961-3697029, Fax: +39-0961-3697341.

Key points

- First-in-class MIR17PTi enables a “one shot” downregulation of the entire miR-17-92 cluster *in vitro* and *in vivo*, with favorable PK profile.
- MIR17PTi affects homeostatic MYC / miR-17-92 feedforward loops in MM cells, resulting in a strong anti-MM activity.

Abstract

The microRNA cluster miR-17-92 is oncogenic and represents a valuable therapeutic target in c-MYC (MYC)-driven malignancies. Here, we developed novel LNA gapmeR antisense oligonucleotides (ASOs) to induce RNase H-mediated degradation of MIR17HG primary transcripts and, consequently, to prevent biogenesis of miR-17-92 microRNAs (miR-17-92s). The leading LNA-ASO, named MIR17PTi, impaired proliferation of several cancer cell lines (n=48) established from both solid and hematologic tumors by on-target antisense activity, and more effectively as compared to miR-17-92*s* inhibitors. By focusing on multiple myeloma (MM), we found that MIR17PTi triggers apoptosis *via* impairment of homeostatic MYC/miR-17-92 feed-forward loops (FFLs) in patient-derived MM cells; and induced MYC-dependent synthetic lethality. We show that alteration of a BIM-centered FFL is instrumental for MIR17PTi to induce cytotoxicity in MM cells. MIR17PTi exerts strong *in vivo* anti-tumor activity in NOD-SCID mice bearing clinically relevant models of MM, with advantageous safety and pharmacokinetics profiles in non-human primates. Altogether, MIR17PTi is a novel pharmacological tool to be tested in early-phase clinical trials against MM and other MYC-driven malignancies.

Introduction

MiR-17-92 is an oncogenic cluster of microRNAs (miRNAs) encoded by *MIR17HG* at 13q31.3[1,2]. According to ENSEMBL genome browser (GRCh38.p10), three long non-coding RNAs (lncRNAs) are produced by the alternative splicing of a MIR17HG primary transcript (MIR17HG-PT), with only lncRNAs MIR17HG-202 and MIR17HG-203 (hereafter simply referred as pri-mir-17-92) generating the six miR-17-92 mature miRNAs (miR-17-92*s*), including miR-17/-18a/-19a/-20a/-19b-1/-92a-1[1,2]. This cluster is steadily upregulated in solid and hematologic malignancies, mainly because of amplification of the genomic locus or by transcriptional mechanisms[1,2]. Based on their seed regions, miR-17-92s are grouped into four different families (*miR-17*, *miR-18*, *miR-19* and *miR-92*), which share most target genes[1,2]. These latter include several tumor suppressors, such as the pro-apoptotic factor BIM (also known as *BCL2L11*), thus explaining the tumor promoting functions of miR-17-92*s*[1,2].

A key transcriptional regulator of *MIR17HG* is the transcription factor c-MYC (MYC)[3]. This oncogene drives the onset and progression of several human malignancies, including multiple myeloma (MM)[4], B-cell lymphomas (BCLs)[5] and triple-negative breast cancer (TNBC)[6], which carry the trait of "hard-to-treat" tumors[7]. miR-17-92 ensures cellular homeostasis during MYC-driven tumorigenesis by counteracting the MYC apoptotic signal. This effect is achieved by the cooperative activity of all six miR-17-92*s*, which coordinately fine-tune MYC expression and suppress MYC-related apoptotic program[3,8]. The close interplay between MYC and miR-17-92, along with the lack of therapeutic tools for the direct targeting of MYC[9], underscores the relevance of miR-17-92 as attractive druggable target in MYC-driven cancer. In this *scenario,* the targeting of miR-17-92 is likely to frame as a MYC-dependent synthetic lethal (SL) approach, whereby it specifically produces cytotoxicity in the presence of hyperactive/deregulated MYC[10].

On these basis, we hypothesized that a powerful anti-tumor effect would be achieved by inducing simultaneous downregulation of all miR-17-92*s*; and we developed a novel strategy that allows their "one shot" inhibition *via* the targeting of miR-17-92 primary transcript by RNase H-activating antisense oligonucleotides (i.e. gapmeRs). Our efforts led to the pre-clinical development as anti-cancer agent of *first-in-class* MIR17PTi (MIR17HG Primary Transcript inhibitor). We demonstrate its therapeutic activity in the context of MM, where MIR17PTi promotes a newly identified MYC-dependent synthetic lethality (SL) *via* the alteration of a BIM-centered MYC-miR-17-92 feed-forward loops (FFLs).

To our knowledge, this is the first report of “pri-miRNA therapeutics” with translational value in human cancer.

Material and Methods

Cells

Human cell lines and primary cells were grown at 37°C, 5% CO_2. Detailed information is included in Supplementary Methods section.

Antisense oligonucleotides, miRNA mimics/inhibitors and shRNAs

The following Long Non-Coding LNA gapmerRs were customly-designed and purchased from Exiqon (Vedbaek, Denmark):

IDS, Sequence and length of seven miR-17-92 LNA gapmeRs and three controls.

IDs	SEQUENCE 5'-3'	LENGHT (mer)
LNA gapmeR_02	ACATCGACACAATAA	15
LNA gapmeR_05	TCAGTAACAGGACAGT	16
LNA gapmeR_06 (MIR17PTi)	TACTTGCTTGGCTT	14
LNA gapmeR_10	ATGCAAAACTAACAGA	16
LNA gapmeR_12	GAAGGAAAATAGCAGGC	16
LNA gapmeR_15	AGCACTCAACATCAGC	16
LNA gapmeR_16	CGACAGGCCGAAGCT	15
Scr-NC (also known as Negative control A)	AACACGTCTATACGC	15
Lp-MIR17PTi	TACTTGCTTGGCTT	14
mix-MIR17PTi	TACTTGCTTGGCTT	14

Detailed information on other oligonucleotides used in our work is reported Supplementary Methods section.

Gymnosis

Cells were seeded at low plating density in order to reach confluence on the final day of the experiments (day 6). Cell number at plating ranged from 0,5 to 2,5 x 10^3 in 96-well plates, from 2,5 to 10 x 10^4 in 12-well plates and from 1 to 3 x 10^5 in 6-well plates.

Transient and stable transfection of cells

Detailed information can be found in Supplementary Methods section.

CRISPR/CAS9-mediated genome editing

Detailed information can be found in Supplementary Methods section.

Survival assay / detection of apoptosis / cell cycle analysis

Detailed information can be found in Supplementary Methods section.

Synergism quantification

Detailed information can be found in Supplementary Methods section.

Reverse transcription (RT) and quantitative real-time amplification (qRT-PCR)

RNA extraction, reverse transcription (RT) and quantitative real-time amplification (qRT-PCR) were performed as previously described[11]. Detailed information is included in Supplementary Methods section.

Western blot analysis

Protein extraction and western blot analysis were performed as previously described[11]. Detailed information is included in Supplementary Methods section.

Confocal Microscopy

Detailed information can be found in Supplementary Methods section.

Gene expression profiling

Detailed information can be found in Supplementary Methods section.

NOD SCID mice and *in vivo* models of human MM

Male CB-17 severe combined immunodeficient (SCID) mice (6- to 8-weeks old; Harlan Laboratories, Inc., Indianapolis) were housed and monitored in our Animal Research Facility. All experimental procedures and protocols had been approved by the Institutional Ethical Committee (Magna Graecia University) and conducted according to protocols approved by the National Directorate of Veterinary Services (Italy). Detailed information can be found in Supplementary Methods section.

Immunohistochemistry (IHC) and in situ hybridization (ISH)

These experiments were performed as recently described by our group[12].

Non-human primates study

These experiments were performed as recently described by our group[12].

Statistical Analysis

All in vitro experiments were repeated at least three times and performed in triplicate; a representative experiment was showed in figures. Statistical significances of differences were determined using Student's t test, with minimal level of significance specified as $p<0.05$. Statistical significance of the in vivo growth inhibition was determined using Student's t test. The minimal level of significance was specified as $p<0.05$. All statistical analyses were determined using GraphPad software (http://www.graphpad.com). Graphs were obtained using GraphPad software.

Results

MIR17PTi prevents biogenesis of miR-17-92*s*

MIR17HG-PT, as well as pri-mir-17-92 , is located within cell nucleus[13]. This environment is selectively enriched of RNase H, an enzyme that catalyzes non-specific cleavage of RNA strands within DNA/RNA hetero-duplexes[14]. We attempted, therefore, to induce degradation of nascent MIR17HG-PT and pri-mir-17-92 by LNA gapmeRs, a highly efficient and recently-developed class of RNase H-activating antisense oligonucleotides (ASOs) (Fig. 1a)[14]. We first screened LNA-modified gapmeRs for their ability to inhibit miR-17-92 cluster in transfected 293T cells: here, among seven original molecules, only gapmeR_06 and gapmeR_15 efficiently downregulated pri-mir-17-92 (Fig. 1b) and all six miR-17-92*s* (Fig. 1c and Supplementary Fig. 1a). Since gapmeR_06 showed higher inhibitory efficiency, it was selected for further development (hereafter named MIR17PTi). Importantly, MIR17PTi downregulated miR-17-92 cluster by activating the RNase H: in fact, chemical modifications of MIR17PTi within the RNase H-recruiting domain (the resulting oligo was named mix-MIR17PTi) abrogated its inhibitory activity (Fig. 1d); consistently, MIR17PTi failed to downregulate pri-mir-17-92 after RNAi-mediated silencing of RNase H1 (Fig. 1e). MIR17PTi also produced the downregulation of lncRNA MIR17HG-201 (Supplementary Fig. 1b), a shorter transcript produced by the alternative splicing of MIR17HG-PT. This isoform does not contain the MIR17PTi-targeted sequence, confirming that MIR17HG-PT is primarily targeted by MIR17PTi.

In transfection-free or “gymnotic” conditions[14], the timing of pri-mir-17-92 downregulation (Fig. 1f) was concomitant with nucleus entrance of a FAM-labeled MIR17PTi (Fig. 1g). We did not observe any further increase of nuclear uptake at day 6 as compared to day 4,5 (not shown), suggesting that the strongest downregulation of pri-mir-17-92 observed at day 6 comes from prolonged activity of MIR17PTi in the nucleus. Importantly, downregulation of pri-mir-17-92 was followed by decrease of miR-17-92*s* (Fig. 1h); both effects (inhibition of pri-mir-17-92 and miR-17-92*s*) occurred in a dose-dependent fashion (Supplementary Fig. 1c-d**)**.

These findings demonstrate that targeting of MIR17HG-PT by LNA gapmeRs prevents the biogenesis of all miR-17-92*s*.

MIR17PTi affects proliferation of several cancer cell lines

We analyzed MIR17PTi activity, by gymnotic exposure, in cancer cells; and we found that it significantly affected the *in vitro* growth of several cancer cell lines (n=48) established

from either solid- or hematologic- tumors (Fig. 2a). Intriguingly, the latter showed the strongest sensitivity to MIR17PTi as well as the highest pri-mir-17-92 expression within the Cancer Cell Line Encyclopedia (Supplementary Fig. 2a). MIR17PTi did not affect the proliferation of four out of five non-malignant cell lines (NM-CLs) (Fig. 2a): indeed, proliferation of THLE-2 (liver) and HK-2 (kidney) NM-CLs was not significantly affected even at concentrations up to five folds higher (50μM) than those used in this screening phase (10μM) (Supplementary Fig. 3a). By qRT-PCR analysis, we found that MIR17PTi efficiently downregulated pri-mir-17-92 and miR-17-92*s* both in MIR17PTi-sensitive and in MIR17PTi-resistant cells, indicating that MIR17PTi resistance did not depend on inefficient uptake of the oligo (Supplementary Fig. 3b-c). Moreover, we further confirmed this pattern of sensitivity/resistance to MIR17PTi by transfecting a subset of both CCLs and NM-CLs (Supplementary Fig. 3d). In CCLs, mix-MIR17PTi did not affect proliferation (Supplementary Fig. 3e) while LNA gapmeR-15, which downregulates both pri-mir-17-92 and miR-17-92*s*, performed similarly to MIR17PTi (Supplementary Fig. 3f-g).

We next evaluated the anti-cancer activity of MIR17PTi as compared to the individual targeting of miR-17-92*s*. At this end, we transfected different CCLs from hematologic malignancies (n=8) with either MIR17PTi or synthetic inhibitors for each miR-17-92*s*; and we found, as shown in Fig. 2b, that MIR17PTi affected proliferation of all CCLs significantly more efficiently than miR-17-92*s* inhibitors. Importantly, the anti-proliferative activity of MIR17PTi was closely reproduced by co-transfecting all miR-17-92*s* inhibitors (pooled miR-17-92*s* inhibitors; Fig. 2c); and the activity of MIR17PTi was significantly rescued by concomitant over-expression of all miR-17-92*s,* by either synthetic mimics or lentivectors (Fig. 2d).

These findings indicate that cancer cells from different tissues, and especially those of hematologic origin, are sensitive to MIR17PTi. Moreover, they strengthen the rational of targeting the entire miR-17-92 cluster *via* MIR17HG-PT degradation instead of inhibiting individual mature miRNA components.

MIR17PTi is highly active in primary MM cells and human myeloma cell lines

Further investigation, to establish proof of concept for the potential therapeutic value of MIR17PTi, was carried out using MM as working platform. In MM patients, by querying a proprietary microarray dataset, we found that expression of pri-mir-17-92 and miR-17-92*s* is significantly upregulated at the most advanced stage (namely secondary plasma cell leukemia, sPCL) (Supplementary Fig. 4a). RNA-seq analysis of 320 newly-

diagnosed MM patients, from IFM/DFCI 2009 clinical study (NCT0191060)[15], indicated that high pri-mir-17-92 expression correlates with worse clinical outcome (OS and PFS) (Supplementary Fig. 4b), even if at this stage it is not significantly upregulated as compared to healthy donors (n=16) (not shown). These data suggested that, in MM patients, higher miR-17-92 expression is associated with a more aggressive phenotype, such as end-stage disease (sPCL) and/or poor prognosis subgroups yet to be defined.

In HMCLs, we found that MIR17PTI affected proliferation in dose-dependent fashion (Fig. 3a); and the timing of this effect overlapped with downregulation of miR-17-92*s* (Fig.3b). Growth-inhibition was ascribed to G_0/G_1 cell cycle arrest (Fig. 3c and Supplementary Fig. 5), apoptosis (Fig.3c and Supplementary Fig. 6 and 7) and senescence (Fig. 3d); and was even more evident in methylcellulose-based long-term cultures, where the growth of colonies was abrogated at nanomolar concentrations (Fig. 3e). Importantly, MIR17PTi was still active against HMCLs made resistant to conventional anti-MM agents, such as dexamethasone (MM.1R), melphalan (LR7), bortezomib (ABZB) or carfilzomib (ACFZ) (Fig. 3f); and survival signals from co-cultured human bone marrow stromal cells (hBMSCs) did not rescue MIR17PTi activity (Fig. 3g and Supplementary Figure 8a). Moreover, combination of MIR17PTi with dexamethasone, melphalan or bortezomib produced in most cases synergistic effects (Fig. 3h and Supplementary Fig. 8b).

In *ex-vivo* viability assays, MIR17PTi was cytotoxic to primary MM (pMM) cells derived from patients at either bone marrow microenvironment (BMM)-dependent (n=11) or BMM-independent (n=2) stage of disease (Fig. 3i; detailed information on pMM cells are reported in Supplementary Fig. 9a). Consistently with a tumor-selective killing activity, MIR17PTi did not affect viability of either CD138+ cells from patients with the pre-malignant condition of monoclonal gammopathy of undetermined significance (MGUS) (n=3) (Supplementary Fig. 9b) nor PBMCs from healthy donors (n=2) (Supplementary Fig. 9c).

These data highlight the strong therapeutic potential of MIR17PTi against MM.

MIR17PTi affects MYC transcriptional network in primary MM cells

By microarray-based gene expression profiling (GEP), we explored the molecular perturbations produced by MIR17PTi in pMM cells (n=4; pt#5, pt#6, pt#7, pt#9) co-cultured with HS-5 stromal cells. Unsupervised hierarchical clustering segregated samples based on treatment, suggesting a coherent transcriptome modulation (figure 4a). Ingenuity

Pathway Analysis (IPA) of GEP data highlighted MYC as the most significantly affected upstream regulator ($p=3,17^{E-06}$, not shown). Consistently, gene set enrichment analysis (GSEA)[16,17] identified MYC_TARGET_V1 as the most significantly enriched Hallmark collection in the positive phenotype (i.e. genes upregulated by MIR17PTi) (Fig. 4b); and in-depth analysis of the MYC_TARGET_V1 founder gene sets (n=404) showed the specific enrichment of transcriptional signatures of MYC-upregulated target genes (Fig. 4c). MIR17PTi induced similar transcriptional alterations in the highly-sensitive AMO1 cells (Supplementary Fig. 10b-c). Conversely, treatment of MIR17PTi-resistant pMM cells (n=2; pt#10, pt#11) did not alter the MYC transcriptional signaling, as assessed by GEP analysis, even if pri-mir-17-92 was significantly downregulated (not shown).

To address the transcriptional changes directly produced in pMM cells after miR-17-92*s* downregulation, we searched for miR-17-92*s* targets among the genes upregulated by MIR17PTi. At this aim, GEP data from MIR17PTi-sensitive pMM cells were matched with computationally predicted and CLIP-seq validated direct interactors of miR-17-92*s* (Fig. 4d). This approach disclosed several upregulated genes (n=65) which are *bona fide* targets of miR-17-92*s* in pMM cells (Fig. 4d and Supplementary Table S1); and, consistently with a direct regulation by miR-17-92*s*, transduction of AMO1 or U266 with a miR-17-92*s* lentiviral vector produced the downregulation of some of these genes (Supplementary Fig. 11a-d). Importantly, approximately the half of these miR-17-92*s* direct targets presents MYC binding loci within the promoter region (28/65), and some have been already validated as transcriptional targets of MYC (15/65), even in B cells (13/65)[18-22] (Fig. 4e and Supplementary Table S1). GEP data were validated in pMM cells (pt#4, pt#5, pt#6) by qRT-PCR analysis of *BIM*, *BZW2*, *DUSP2*, *NAP1L1* and *VDAC1* (Fig. 4f) and in AMO1 either by qRT-PCR or western blotting (Supplementary Fig. 11e-f).

These findings suggested that MIR17PTi upregulates a subset of genes which are transcriptionally regulated by MYC, pointing to the existence of a MYC/miR-17-92 co-regulated network that might exert homeostatic functions in MM cells; and led us to hypothesize that MIR17PTi exerts its anti-MM activity *via* the redirection of a MYC-related transcriptional program towards apoptotic cell death.

MIR17PTi triggers MYC-dependent synthetic lethality

We investigated whether an active MYC transcriptional program sensitizes MM cells to MIR17PTi; at this aim, we transduced MYC defective U266[11] with a lentiviral vector carrying the MYC open reading frame ($U266^{MYC+}$) or with an empty vector ($U266^{MYC-}$).

Both pri-mir-17-92 and miR-17-92*s* increased in U266^{MYC+} (Supplementary Fig. 12a), which is consistent with a MYC upstream regulation on *MIR17HG* also in MM cells. This assumption was further corroborated by the *in silico* analysis of a proprietary microarray dataset (GSE70323) that showed positive correlation between *MYC* and *MIR17HG* in MM patients (Supplementary Fig. 12b). More importantly, MIR17PTi was considerably more cytotoxic to U266^{MYC+} as compared to U266^{MYC-} (Fig. 5a), supporting the idea that MIR17PTi triggers a MYC-dependent synthetic lethality (SL) in MM cells.

We next explored MIR17PTi activity in P493-6 and MYC-ER HMECs cells, where MYC expression can be conditionally modulated. Specifically, P493-6 is an immortalized B-cell line carrying a tetracycline-regulated *MYC*[23], while MYC-ER HMEC is an immortalized human mammary epithelial cell line engineered with an inducible MYC and estrogen receptor fusion protein (MYC-ER)[24]. These cells represent valuable experimental models of B-cell lymphomas (BCLs) and triple-negative breast cancer (TNBC), respectively, which are prototypical MYC-driven diseases[5,6] where miR-17-92 is commonly upregulated[25,26]. Both pri-mir-17-92 and miR-17-92*s* increased in P493-6 and MYC-ER HMECs when MYC expression or activity, respectively, was turned *on* (Supplementary Fig. 12a). Again, treatment with MIR17PTi effectively induced cell death only at MYC-*on* cells, without any significant cytotoxicity when MYC was silenced or inactive (Fig. 5a).

These data provide the formal proof that treatment with MIR17PTi is a new MYC-dependent SL approach in MM and other cancers.

Impairment of a BIM-centered MYC/miR-17-92 FFL mediates MIR17PTi anti-MM activity

To shed light on the molecular mechanisms underlying MYC-dependent SL by MIR17PTi, we next focused on MYC/miR-17-92*s* co-regulated targets in MM cells; and, among them, the tumor-suppressor and pro-apoptotic factor BIM, a BH3-only BCL2-family member, appeared of particular interest. In fact, MYC positively regulates *BIM* transcription[27] while different miR-17-92*s* repress its expression at post-transcriptional level[1-3], thus forming a prototypical miRNA-mediated FFL[28]. Moreover, BIM is the primary effector of MYC-induced apoptotic program in MYC-overexpressing cells[27], with haplo-insufficient tumor-suppressor activity in B cells[18,27]. Interestingly, OPM-2 and SK-MM-1, which were the only two MIR17PTi-resistant HMCLs, did not express detectable levels of BIM protein (Fig. 5b) or mRNA (not shown), likely due to epigenetic repression of its transcription (in fact, either OPM-2 nor SK-MM-1 bring deletion of BCL2L11/BIM; not shown). In hdPBMCs, which

express very low levels of BIM protein as compared to HMCLs (Fig. 5b and Supplementary Fig. 13), MIR17PTi did not increase BIM expression (Supplementary Fig. 13). On the other hand, MIR17PTi strongly upregulated BIM protein in pMM cells (Fig. 5c) and different HMCLs (Fig. 5d); upregulation of BIM was also produced by co-transfection of pooled miR-17-92s inhibitors (Fig. 5e), while its protein expression was significantly reduced in AMO1 transduced with a miR-17-92*s* lenti-vector (Fig. 5f). More importantly, CRISPR/Cas9-mediated knock-out of BIM strongly antagonized MIR17PTi-mediated killing in both AMO1 ($AMO1^{BIM-}$) and $U266^{MYC+/BIM-}$ generated clones (Fig. 5g-h).

These results demonstrate that MIR17PTi triggers MYC-dependent SL in MM cells, in a significant part, *via* the impairment of a BIM-centered MYC/miR-17-92 FFL, which results in the upregulation of BIM up to pro-apoptotic level (Fig. 5i). Of course, upregulation of other miR-17-92*s* targets likely contributes to its activity; indeed, MIR17PTi also increased the expression of relevant tumor-suppressors such as CDKN1A (also known as p21), TP53, E2F1 or PTEN (Supplementary Fig. 13) which are validated targets of different miR-17-92*s*[2].

In vivo anti-MM activity of MIR17PTi in NOD SCID mice

We investigated the *in vivo* activity of MIR17PTi in NOD SCID mice bearing subcutaneous (s.c.) MM xenografts (NCI-H929, $AMO1^{luc+}$ and bortezomib-refractory $ABZB^{luc+}$). Importantly, systemic administration (i.v.) of naked MIR17PTi significantly inhibited tumor-growth (Fig. 6a; supporting BLI images are reported in Supplementary Fig. 14a-b) and prolonged animal survival (Fig. 6b), with a well-defined therapeutic window (H&E staining of accumulation organs is reported in Supplementary Fig. 15a). qRT-PCR analysis of pri-mir-17-92 confirmed a productive antisense activity of MIR17PTi in retrieved tumors (Fig. 6c), which also resulted in BIM upregulation at both mRNA and protein level (Fig. 6d). By *in situ* hybridization (ISH) analysis, using a specific LNA probe for MIR17PTi, we showed a higher uptake in kidney and liver, followed by BM, heart and lung (Supplementary Fig. 15b), which is consistent with canonical LNA-modified ASO pharmacokinetics (PK)[29]. By this approach, MIR17PTi was also detected in retrieved tumors (Supplementary Figure 15b). Next, we investigated the anti-MM activity of MIR17PTi in the clinically-relevant SCID-*hu* model[30], which allows the *in vivo* growth of BM-dependent MM cells within a recapitulated human bone marrow *milieu*: in this model, MIR17PTi elicited a strong anti-MM activity, as assessed by measurement of soluble IL-6R levels in the plasma of treated vs untreated mice (Fig. 6e).

These data demonstrate a relevant *in vivo* anti-MM activity of MIR17PTi as single agent, even capable to overcome the protective effects of the bone marrow *milieu*.

Safety and PK profile of MIR17PTi in non-human primates

We investigated the safety and plasmatic pharmacokinetics (PK) of MIR17PTi in non-human primates (non-naïve cynomolgus monkeys). The amount per injection was equivalent to the amount administered to NOD SCID mice, after inter-species dose conversion[31]. To assess the safety profile, MIR17PTi was injected on days 1-4-8-15-22 (same schedule used in mice) and, as control, an additional animal was i.v. injected with saline solution. At the end of treatment period, no signs of toxicity could be recorded (Supplementary Fig. 16-17). MIR17PTi was then i.v. injected as single dose in a third animal, in order to explore the plasmatic PK profile. Plasma was collected at following time-points: pre-dose, 0.5 hr, 1 hr, 2 hrs, 4 hrs, 6 hrs, 12 hrs, 24 hrs and 48 hrs. Plasmatic MIR17PTi, as detected by PNA-HPCL assay, peaked at a T_{max} of 0.5 hr with a C_{max} of 2,638 ng/mL (Fig. 7a). Compared with the 28,473 hr * ng/mL value of area under the concentration-time curve ($AUC_{0-\infty}$), the 21,994 hr * ng/mL value of AUC_{0-12} indicated that more than 75% of MIR17PTi left the plasma within 12 hrs (Fig. 7b). These findings were consistent with the favorable PK profile of LNA-modified ASOs, which assumes rapid plasmatic clearance *via* tissue uptake[12,29].

Discussion

We developed and here described a new strategy for the therapeutic targeting of miRNA network in human cancer. This approach exploits RNase H-activating LNA gapmeRs to induce the degradation of miRNA primary transcripts (pri-miRNA) and, consequently, to prevent the biogenesis of related mature miRNAs. Recent evidence demonstrated that these third-generation ASOs predominantly act on nascent primary transcripts (nascent pri-miRNAs in this study) before being processed by the splicing machinery[32,33]. As compared to canonical miRNA inhibitors, LNA gapmeRs better adapt to the targeting of miRNA clusters: in this case, indeed, degradation of pri-miRNAs leads to the concomitant downregulation of all miRNA members of the cluster. On these premises, we identified the miR-17-92 cluster as a target with high translational value in the context of human cancer[3]; and, among different originally-designed LNA gapmeRs, we selected MIR17PTi for its antisense activity. Consistent with our initial hypothesis, MIR17PTi efficiently downregulates pri-mir-17-92 and all miR-17-92*s* in RNase H-dependent manner; by contrast, we failed to induce these effects *via* RNAi, possibly due to the absence or alternative functions of RNAi machinery within cell nucleus[34,35]. Our study spanned from conceptual drug design to pre-clinical investigation in non-human primates.

Previous reports suggested that oncogenicity of miR-17-92 may be confined to one or few miRNAs in specific cellular contexts[36], thus supporting the rational design of miR-17-92*s*-based therapeutic strategies. Our data, indeed, confirm that CCLs may be differently addicted to miR-17-92 members; however, they rather support the potential advantage of concomitant downregulation of the entire cluster at least in hematologic cancers. In fact, MIR17PTi antagonized the proliferation of hematologic CCLs more efficiently than synthetic inhibitors of miR-17-92*s*. Moreover, hematologic CCLs from the same malignancy such as MCL or MM were differently sensitive to the inhibition of each miR-17-92*s*, making very likely the failure of a miRNA-based therapeutic approach in the context of the intra-/inter-clonal heterogeneity which features human cancer[37,38]. Actually, our results can be explained taking into account that miR-17-92*s* have redundant functions because of the sharing of most of the mRNA targets: it is reasonable that, upon individual antagonism of each cluster member, the remaining miR-17-92*s* could act by compensatory mechanisms. Moreover, it must be noted that MIR17PTi also induces the downregulation of lncRNAs MIR17HG-201/-202/-203, pre-mir-17-92*s* (pre-mir-17/-18a/-19a/-20a/-19b/-92a) and miR-17-92*s* complementary strands (miR-17-3p/ miR-18a-3p/ miR-19a-5p/ miR-20a-3p/ miR-19b-5p/ miR-92a-5p) that are potentially endowed with own functions; and

can contribute to MIR17PTi anti-cancer activity. This possibility is also suggested by the incomplete rescue obtained by enforcing the expression of all miR-17-92*s*. However, this point has not been addressed in our work and requires further investigation.

We used MM, a MYC-driven malignancy of terminally-differentiated B cells (i.e. plasma cells)[39], as the main investigational platform for the pre-clinical development of MIR17PTi. In a proprietary RNA-seq dataset of 320 newly-diagnosed MM patients, we disclosed the association of high pri-mir-17-92 levels with worse clinical outcome. *In vitro*, MIR17PTi efficiently killed HMCLs and pMM cells, even co-cultured with hBMSCs and/or HS-5. At molecular level, we found that the induction of a MYC-related and pro-apoptotic transcriptional network underlies the anti-MM activity of MIR17PTi. We explained this outcome by hypothesizing that MIR17PTi impairs a functional interplay between MYC and miR-17-92, which follows the general scheme of homeostatic miRNA-mediated FFLs[28,40]; and we formally proved our hypothesis by demonstrating that an active MYC downstream signaling, achieved by enforcing MYC expression (U266^{MYC+} or P493-6^{DOX-}) or activity (MYC-ER HMEC^{TAM+}), strongly sensitizes to MIR17PTi killing. We explored the molecular mechanisms underlying this synthetic lethal effect in MM cells by focusing on MYC/miR-17-92*s* co-regulated targets. Specifically, the tumor suppressor BIM gained our attention given its established role as the primary effector of MYC apoptotic program[18,27]. The finding that MIR17PTi-resistant MM cells (i.e OPM2 and SK-MM-1) did not express detectable BIM protein/mRNA prompted us to investigate MIR17PTi activity in HMCLs after BIM knock-out (i.e. AMO1^{BIM-} and U266$^{MYC+/BIM-}$); and in these experimental conditions the killing activity of MIR17PTI was strongly antagonized. On these basis, we speculate that MYC/miR-17-92 FFLs are required to maintain the expression of BIM, and likely other co-regulated genes, at homeostatic levels that allow MM cells to proliferate; and we conclude that MIR17PTi triggers MYC-dependent synthetic lethality by affecting these homeostatic FFLs, resulting in the upregulation of BIM (and likely other genes) over a homeostatic threshold at levels prompting MM cells towards apoptosis. Overall, this mechanism is likely to occur specifically in cancer cells, where oncogenic MYC controls the transcription of apoptotic genes; it is known, in fact, that this transcriptional activity is not relevant when MYC is expressed within a physiologic range[41].

MIR17PTi antagonized *in vivo* growth of human MM cells as single agent. This was demonstrated in four different and clinically relevant murine models, including those refractory to conventional anti-MM agents (ABZB) and those in which MM cells grow within a recapitulated human bone marrow microenvironment (i.e. SCID-*hu*)[30]. Moreover, the

potential therapeutic benefit of treatment with MIR17PTi was further corroborated by its synergistic anti-MM activity in combination with conventional and clinically-active agents, such as dexamethasone, melphalan or bortezomib. These data indeed provide the rational framework for the design of novel MIR17PTi-based drug combinations for the treatment of MM patients.

To our knowledge this is the first report of pri-miRNA therapeutics with translational value for cancer therapy. We believe that this study opens a new avenue for targeting the miRNA network in human cancer, and provides with MIR17PTi a powerful weapon against MM and other hard-to-treat MYC-driven tumors.

Author Contributions: E.M., L.B. and C.F. conducted most *in vitro* and *in vivo* experiments. E.M. and A.G. performed experiments with SCID-*hu* animal model. M.T.D.M., L.B. and F.S. performed gene expression profiling (E.M. analyzed GEP data). M.E.G.C. performed drug combination studies and analyzed data with CalcuSyn. M.M. conducted bioinformatic analysis of gene and miRNA expression in MM patients. M.K.S. analyzed RNA-seq data. M.A.S. performed methylcellulose assay. M.R.P. performed confocal microscopy analysis. S.S. performed electron microscopy analysis. M.T.F. established U266^{MYC+} cells and contributed to interpretation of data. N.M.F. suggested the use of LNA gapmeRs to target the miR-17-92 cluster and contributed to the design and interpretation of key experiments. N.A. and M.R. contributed to the design and interpretation of key experiments. A.N. and N.C.M. provided reagents and contributed to interpretation of data. All authors read and edited the manuscript. E.M., P.T. and P.T. designed research studies and wrote the manuscript.

References

1. Concepcion CP, Bonetti C, Ventura A. The microRNA-17-92 family of microRNA clusters in development and disease. *Cancer J*. 2012;18(3):262-267.
2. Mogilyansky E, Rigoutsos I. The miR-17/92 cluster: a comprehensive update on its genomics, genetics, functions and increasingly important and numerous roles in health and disease. *Cell Death Differ*. 2013;20(12):1603-1614.
3. He L, Thomson JM, Hemann MT, et al. A microRNA polycistron as a potential human oncogene. *Nature*. 2005;435(7043):828-833.
4. Chesi M, Robbiani DF, Sebag M, et al. AID-dependent activation of a MYC transgene induces multiple myeloma in a conditional mouse model of post-germinal center malignancies. *Cancer Cell*. 2008;13(2):167-180.
5. Ott G, Rosenwald A, Campo E. Understanding MYC-driven aggressive B-cell lymphomas: pathogenesis and classification. *Blood*. 2013;122(24):3884-3891.
6. Horiuchi D, Kusdra L, Huskey NE, et al. MYC pathway activation in triple-negative breast cancer is synthetic lethal with CDK inhibition. *J Exp Med*. 2012;209(4):679-696.
7. Wall M, Poortinga G, Stanley KL, et al. The mTORC1 inhibitor everolimus prevents and treats Emu-Myc lymphoma by restoring oncogene-induced senescence. *Cancer Discov*. 2013;3(1):82-95.
8. Mihailovich M, Bremang M, Spadotto V, et al. miR-17-92 fine-tunes MYC expression and function to ensure optimal B cell lymphoma growth. *Nat Commun*. 2015;6:8725.
9. Stine ZE, Dang CV. Splicing and Dicing MYC-Mediated Synthetic Lethality. *Cancer Cell*. 2015;28(4):405-406.
10. Wang Y, Engels IH, Knee DA, Nasoff M, Deveraux QL, Quon KC. Synthetic lethal targeting of MYC by activation of the DR5 death receptor pathway. *Cancer Cell*. 2004;5(5):501-512.
11. Morelli E, Leone E, Cantafio ME, et al. Selective targeting of IRF4 by synthetic microRNA-125b-5p mimics induces anti-multiple myeloma activity in vitro and in vivo. *Leukemia*. 2015;29(11):2173-2183.
12. Gallo Cantafio ME, Nielsen BS, Mignogna C, et al. Pharmacokinetics and Pharmacodynamics of a 13-mer LNA-inhibitor-miR-221 in Mice and Non-human Primates. *Mol Ther Nucleic Acids*. 2016;5(6).
13. Olive V, Li Q, He L. mir-17-92: a polycistronic oncomir with pleiotropic functions. *Immunol Rev*. 2013;253(1):158-166.
14. Stein CA, Hansen JB, Lai J, et al. Efficient gene silencing by delivery of locked nucleic acid antisense oligonucleotides, unassisted by transfection reagents. *Nucleic Acids Res*. 2010;38(1):e3.
15. Attal M, Lauwers-Cances V, Hulin C, et al. Lenalidomide, Bortezomib, and Dexamethasone with Transplantation for Myeloma. *N Engl J Med*. 2017;376(14):1311-1320.
16. Liberzon A, Birger C, Thorvaldsdottir H, Ghandi M, Mesirov JP, Tamayo P. The Molecular Signatures Database (MSigDB) hallmark gene set collection. *Cell Syst*. 2015;1(6):417-425.
17. Subramanian A, Tamayo P, Mootha VK, et al. Gene set enrichment analysis: a knowledge-based approach for interpreting genome-wide expression profiles. *Proc Natl Acad Sci U S A*. 2005;102(43):15545-15550.
18. Egle A, Harris AW, Bouillet P, Cory S. Bim is a suppressor of Myc-induced mouse B cell leukemia. *Proc Natl Acad Sci U S A*. 2004;101(16):6164-6169.
19. Golomb L, Bublik DR, Wilder S, et al. Importin 7 and exportin 1 link c-Myc and p53 to regulation of ribosomal biogenesis. *Mol Cell*. 2012;45(2):222-232.
20. Li Z, Van Calcar S, Qu C, Cavenee WK, Zhang MQ, Ren B. A global transcriptional regulatory role for c-Myc in Burkitt's lymphoma cells. *Proc Natl Acad Sci U S A*. 2003;100(14):8164-8169.
21. Wu CH, Sahoo D, Arvanitis C, Bradon N, Dill DL, Felsher DW. Combined analysis of murine and human microarrays and ChIP analysis reveals genes associated with the ability of MYC to maintain tumorigenesis. *PLoS Genet*. 2008;4(6):e1000090.
22. Zeller KI, Zhao X, Lee CW, et al. Global mapping of c-Myc binding sites and target gene networks in human B cells. *Proc Natl Acad Sci U S A*. 2006;103(47):17834-17839.
23. Schuhmacher M, Staege MS, Pajic A, et al. Control of cell growth by c-Myc in the absence of cell division. *Curr Biol*. 1999;9(21):1255-1258.

24. Kessler JD, Kahle KT, Sun T, et al. A SUMOylation-dependent transcriptional subprogram is required for Myc-driven tumorigenesis. *Science*. 2012;335(6066):348-353.
25. de Rinaldis E, Gazinska P, Mera A, et al. Integrated genomic analysis of triple-negative breast cancers reveals novel microRNAs associated with clinical and molecular phenotypes and sheds light on the pathways they control. *BMC Genomics*. 2013;14:643.
26. Dal Bo M, Bomben R, Hernandez L, Gattei V. The MYC/miR-17-92 axis in lymphoproliferative disorders: A common pathway with therapeutic potential. *Oncotarget*. 2015;6(23):19381-19392.
27. Muthalagu N, Junttila MR, Wiese KE, et al. BIM is the primary mediator of MYC-induced apoptosis in multiple solid tissues. *Cell Rep*. 2014;8(5):1347-1353.
28. Tsang J, Zhu J, van Oudenaarden A. MicroRNA-mediated feedback and feedforward loops are recurrent network motifs in mammals. *Mol Cell*. 2007;26(5):753-767.
29. Geary RS, Norris D, Yu R, Bennett CF. Pharmacokinetics, biodistribution and cell uptake of antisense oligonucleotides. *Adv Drug Deliv Rev*. 2015;87:46-51.
30. Tassone P, Neri P, Carrasco DR, et al. A clinically relevant SCID-hu in vivo model of human multiple myeloma. *Blood*. 2005;106(2):713-716.
31. Nair AB, Jacob S. A simple practice guide for dose conversion between animals and human. *J Basic Clin Pharm*. 2016;7(2):27-31.
32. Kamola PJ, Kitson JD, Turner G, et al. In silico and in vitro evaluation of exonic and intronic off-target effects form a critical element of therapeutic ASO gapmer optimization. *Nucleic Acids Res*. 2015;43(18):8638-8650.
33. Kasuya T, Hori S, Watanabe A, et al. Ribonuclease H1-dependent hepatotoxicity caused by locked nucleic acid-modified gapmer antisense oligonucleotides. *Sci Rep*. 2016;6:30377.
34. Castel SE, Martienssen RA. RNA interference in the nucleus: roles for small RNAs in transcription, epigenetics and beyond. *Nature Reviews Genetics*. 2013;14(2):100-112.
35. Zeng Y, Cullen BR. RNA interference in human cells is restricted to the cytoplasm. *RNA*. 2002;8(7):855-860.
36. Olive V, Bennett MJ, Walker JC, et al. miR-19 is a key oncogenic component of mir-17-92. *Genes Dev*. 2009;23(24):2839-2849.
37. Tirosh I, Izar B, Prakadan SM, et al. Dissecting the multicellular ecosystem of metastatic melanoma by single-cell RNA-seq. *Science*. 2016;352(6282):189-196.
38. Bolli N, Avet-Loiseau H, Wedge DC, et al. Heterogeneity of genomic evolution and mutational profiles in multiple myeloma. *Nat Commun*. 2014;5:2997.
39. Munshi NC, Anderson KC. New strategies in the treatment of multiple myeloma. *Clin Cancer Res*. 2013;19(13):3337-3344.
40. Martinez NJ, Walhout AJ. The interplay between transcription factors and microRNAs in genome-scale regulatory networks. *Bioessays*. 2009;31(4):435-445.
41. Dang CV. A Time for MYC: Metabolism and Therapy. *Cold Spring Harb Symp Quant Biol*. 2016;81:79-83.

Acknowledgments: We thank Dr. Dirk Eick (Helmholtz-Zentrum München, Molecular Epigenetics), Dr. Stephen J. Elledge (Harvard Medical School, Division of Genetics, Brigham and Women's Hospital) and Dr. Christoph Driessen (Cantonal Hospital St Gallen, St Gallen, Switzerland) for providing us relevant cellular models. We thank Dr. Emilia Dora Giovannone and Dr. Valter Agosti for kindly help in the generation of genome-edited cell lines (i.e. cell sorting and single-cell plating). We thank Dr. Ivana Criniti (Magna Graecia University, Catanzaro, Italy) for editorial assistance.

Financial support: This work has been mainly supported by the Italian Association for Cancer Research (AIRC) with “Special Program for Molecular Clinical Oncology–5 per mille”, 2010/15 and its Extension Program” No. 9980, 2016/18 (PI: PT); and also by “Innovative Immunotherapeutic Treatments of Human Cancer” Multi Unit Regional No. 16695 (co-financed by AIRC and the CARICAL foundation). This work has also been partially supported by grants from NIH P50-100707 (NCM); by grants from NIH P01-155258/07 (NCM and MTF); and by grants from AIRC IG1 6722 (AN).

Competing interests: N.M.F. is an employee of Exiqon. The other authors declare no competing financial interests.

Figures & Figure legends

Fig. 1. Development of MIR17PTi

(**a**) Cartoon summarizing the activity of LNA gapmeRs on miR-17-92 cluster.

(**b**) qRT-PCR analysis of pri-mir-17-92 expression in 293T two days after transfection with miR-17-92 LNA gapmeRs or scr-NC (25nM).

(**c**) qRT-PCR analysis of miR-17-92*s* in 293T two days after transfection with mir-17-92 LNA gapmeRs or scr-NC (25nM).

(**d**) qRT-PCR analysis of pri-mir-17-92 expression in 293T two days after transfection with mix-MIR17PTi or scr-NC (25nM).

(**e**) qRT-PCR analysis of pri-mir-17-92 (left) and western blotting of RNASE H1 (right) in 293T co-transfected with either siRNAs targeting RNASE H1 (siRNASE H1, 25nM) or scrambled siRNAs (siCNT, 25nM) and MIR17PTi or scr-NC (25nM) (three days time point). The results of qRT-PCR analysis are average pri-mir-17-92 expression levels after normalization with GAPDH and ΔΔCt calculations. GAPDH was used as protein loading control.

(**f**) qRT-PCR analysis of pri-mir-17-92 in 293T during a time-course exposure (day 1,5-3-4,5-6, every 36 hours) to MIR17PTi or scr-NC (10µM). The results are average expression levels after normalization with GAPDH and ΔΔCt calculations.

(**g**) Confocal microscopy analysis of 293T after three days or four days and half of exposure to FAM-labeled MIR17PTi (10µM). Cell nuclei are evidenced by DAPI staining.

(**h**) qRT-PCR analysis of miR-17-92*s* in 293T during a time-course exposure (day 1,5-3-4,5-6, every 36 hours)) to MIR17PTi or scr-NC (10µM). The results are average expression levels after normalization with RNU44 and ΔΔCt calculations.

Data from 1 out of 3 independent experiments is shown in each panel. **indicates p<0.0*

Fig. 2. In vitro anti-cancer activity of MIR17PTi

(**a**) CCK-8 assay of cancer cell lines (CCLs, n=48) and non-malignant cell lines (NM-CLs, n=5) exposed for six days to MIR17PTi or scr-NC (10µM). Data are represented as percentage of MIR17PTi-treated live cells (absorbance), as compared to scr-NC. Dashed lines indicate 20% (upper line) and 80% (bottom line) growth inhibition.

(**b**) CCK-8 proliferation assay of eight CCLs (P3HR1 (DLBCL); SULTAN (BL); JeKo-1, Maver (MCL); AMO1, KMS-12-BM, NCI-H929, RPMI-8226 (MM)) transfected with indicated miRNA inhibitors or MIR17PTi (25nM). Data are represented as compared (percentage) to live cells after scr-NC transfection.

(**c**) CCK-8 proliferation assay of RPMI-8226 and AMO1 after transfection with miR-NC-inhibitors (150nM) or pooled miR-17-92*s* inhibitors (25nM each) or scr-NC (25nM) or MIR17PTi (25nM). Data are represented as compared (percentage) to live cells after mock (RNase-free water) transfection.

(**d**) CCK-8 proliferation assay of: (left panel) AMO1 two days after co-transfection with scr-NC (5nM or 25nM; showed as single point since no difference was detected in percentage of live cells) or MIR17PTi (5nM or 25nM) and miR-NC-mimics (60nM) or pooled miR-17-92*s* mimics (10nM each); (right panel) AMO1 transduced with an empty lentiviral vector or a miR-17-92*s* lentiviral vector and then exposed for six days to scr-NC or MIR17PTi (0.5µM).

Data from 1 out of 3 independent experiments is shown in each panel. **indicates* $p<0.05$

NM-CLs= non malignant cell lines; NSCLC= non small cell lung cancer; BC= breast cancer; PC= pancreatic cancer; MPM= malignant pleural mesothelioma; AML= acute myeloid leukemia; TCL= T cell leukemia; BL= Burkitt lymphoma; DLBCL= diffuse large B cell lymphoma; MCL= mantle cell lymphoma; MM= multiple myeloma.

Fig. 3. *In vitro* activity of MIR17PTi in HMCLs and pMM cells

(**a**) Dose-dependent activity of MIR17PTi (six days time point) in HMCLs (n=10) as assessed by CCK-8 proliferation assay. Live cells are represented as compared (percentage) to untreated controls.

(**b**) Time-dependent activity of MIR17PTi (1µM) in AMO1, as assessed by qRT-PCR analysis of (left panel) pri-mir-17-92 and (mid panel) miR-17-92*s*. The results shown are average pri-mir-17-92 or miRNAs expression levels after normalization with GAPDH or RNU44 and ΔΔCt calculation (expressed as percentage). Time-dependent activity of MIR17PTi (1µM) in AMO1, as assessed by CCK-8 assay (right pane).

(**c**) Cell cycle analysis of AMO1 exposed for six days to MIR17PTi (1 µM) or sc-NC (1 µM).

(**d**) Flow cytometry analysis of senescent AMO1 cells (β-Galactosidase positive) exposed for six days to MIR17PTi (1µM) o scr-NC (1µM).

(**e**) Methylcellulose clonogenic assay of AMO1 exposed to MIR17PTi (1µM) o scr-NC (1µM) (two weeks time point).

(**f**) CCK-8 proliferation assay of HMCLs sensitive (MM.1S, U266, AMO1) or resistant (MM.1R, LR7, ABZB, ACFZ) to conventional anti-MM agents (dexamethasone, melphalan, bortezomib, carfilzomib) exposed to different concentrations of MIR17PTi for six days.

(**g**) CCK-8 assay of hBMSCs, AMO1 or AMO1 co-cultured with hBMSCs after six days of exposure to indicated concentrations of MIR17PTi.

(**h**) Table showing combination indexes (CI) resulting from combinatorial treatments of AMO1 with MIR17PTi and dexamethasone or melphalan or bortezomib (six days time point).

(**i**) Flow-cytometry analysis of 7-AAD stained pMM cells (n=13) exposed for eight days to MIR17PTi or scr-NC (2,5µM). pMM cells were cultured adherent to GFP+ HS-5 stromal cells (pt#1-3, patients with intra-medullary disease) or physically separated from HS-5 by membranes (pt#4-11, patients with intra-medullary disease) or alone (pt#12-13, patients with extra-medullary disease at relapse, sPCL). In the lower panel (within the frame) it is represented median activity of MIR17PTi in sensitive pMM cells (n=10) from the left panel.

**indicates p<0.05*

Fig. 4. Molecular perturbation induced by MIR17PTi in pMM cells

(**a**) Hierarchical clustering of pMM cells (n=4, pt#5, pt#6, pt#7, pt#9) exposed for six days to MIR17PTi (2,5 µM) or equimolar scr-NC.

(**b**) Table of gene sets, from the Hallmark collection, enriched of genes upregulated by MIR17PTi (positive phenotype) in sensitive pMM cells (pt#5, pt#6, pt#7, pt#9). Number of genes in each set (size), the normalized enrichment score (NES), and test of statistical significance (FDR q value) are highlighted.

(**c**) Enrichment plots of three representative transcriptional signatures of MYC upregulated target genes in the positive phenotype of sensitive pMM cells exposed to MIR17PTi (2.5µM) for six days.

(**d**) Venn diagram intersecting genes upregulated by MIR17PTi with genes predicted as miR-17-92*s* targets (by miRcode) and genes validated as miR-17-92*s* interactors in CLIP-seq experiments (starBase v2.0).

(**e**) Representation of MYC/miR-17-92 FFLs. In red are reported genes with a fold change (FC) increase >1.5.

(**f**) qRT-PCR analysis of pri-mir-17-92 and *BIM*, *BZW2*, *DUSP2*, *NAP1L1* or *VDAC1* mRNAs in pMM cells (n=3) exposed to MIR17PTi (2.5µM) for six days. The results shown are average pri-mir-17-92 or mRNAs expression levels after normalization with GAPDH and ΔΔCt calculations.

**indicates p<0.05.*

Fig. 5. Molecular mechanism underlying MIR17PTi pro-apoptotic activity

(**a**) 7-AAD flow cytometry assay in: (left panel) U266^{MYC-}/U266^{MYC+} after six days of treatment with MIR17PTi (2,5 µM) or scr-NC (2,5 µM); it is reported western blotting of MYC protein in U266^{MYC-} and U266^{MYC+}. GAPDH was used protein loading control. (mid panel) P493-6 after six days of treatment with MIR17PTi (2,5 µM) or scr-NC (2,5 µM), in presence or absence of doxycycline (dox); it is reported western blotting of MYC protein in P493-6 cultured for two days with or without doxycycline. GAPDH was used protein loading control. (right panel) Trypan blue exclusion staining in MYC-ER HMECs two days after transfection with MIR17PTi (50nM) or scr-NC (50nM), and cultured with or without tamoxifen (tam).

(**b**) Western blotting of BIM in lysates from hdPBMCs (n=2), Jeko-1 (MCL, BIM-null), Daudi, Raji (BL) and indicated HMCLs. GAPDH was used as protein loading control.

(**c**) Western blot analysis of BIM in lysates from pMM cells (pt#12 / #13, extra-medullary MM) exposed to MIR17PTi for six days at indicated concentrations. GAPDH was used as protein loading control.

(**d**) Western blotting of BIM in AMO1, NCI-H929 or INA-6 exposed for six days to MIR17PTi (AMO1=1µM, NCI-H929 and INA-6=2.5µM) or equimolar scr-NC. GAPDH was used as protein loading control.

(**e**) Western blot analysis of BIM in lysates from AMO1 transfected with miR-NC inhibitor (150nM) or pooled miR-17-92*s* inhibitors (25nM each) (two days time point). GAPDH was used as protein loading control.

(**f**) Western blot analysis of BIM in lysates from AMO1 transduced with an empty lentiviral vector or a miR-17-92*s* lentiviral vector. GAPDH was used as protein loading control.

(**g**) Western blot analysis of BIM (upper panel) and flow cytometry analysis of 7-AAD stained cells (lower panel) in CRISPR/CAS9 genome-edited AMO1^{BIM-} cells. GAPDH was used as protein loading control. Flow-cytometry was performed after six days of exposure to MIR17PTi (1µM) o scr-NC (1µM)

(**h**) Western blot analysis of BIM (upper panel) and flow cytometry analysis of 7-AAD stained cells (lower panel) in CRISPR/CAS9 genome-edited U266$^{MYC+/BIM-}$ cells. GAPDH was used as protein loading control. Flow-cytometry was performed after six days of exposure to MIR17PTi (2.5µM) o scr-NC (2.5µM)

(**i**) Proposed model of MYC/miR-17-92 FFLs and MIR17PTi mechanism of action in MM cells. TR=transcriptional regulation; PTR=post-transcriptional regulation.

Data from 1 out of 3 independent experiments is shown in each panel. **indicates p<0.05*

Fig. 6. *In vivo* anti-MM activity of MIR17PTi

(**a**) *In vivo* growth-inhibition of NCI-H929, AMO1^{luc+} or ABZB^{luc+} s.c. xenografts by MIR17PTi (2mg/kg). Treatments were performed on days 1-4-8-15-22 (NCI-H929) or 1-4-8-11 (AMO1^{luc+} and ABZB^{luc+}). Mice were also treated with bortezomib (BZB) as positive control (1mg/kg on days 1-4-8-11). Number of xenografted mice: NCI-H929=17 (NT=7, MIR17PTi=10); AMO1^{luc+}=13 (NT=5, MIR17PTi=5, BZB=3); ABZB^{luc+}=12 (NT=4, MIR17PTi=5, BZB=3). Treatments were performed systemically (i.v.). In figure are reported the tumor volumes at day 33 (NCI-H929) or day 12 (AMO1^{luc+} and ABZB^{luc+}) after the first treatment. Supporting images and BLI measurements are shown in Supplementary Fig. S14.

(**b**) Survival curves (Kaplan–Meier) relative to mice reported in Fig. 6A (log-rank test, P <0.05). Survival was evaluated from the first day of treatment until death or sacrifice. Percentage of mice alive is shown.

(**c**) qRT-PCR analysis of pri-mir-17-92 in retrieved NCI-H929 (n=3) or AMO1^{luc+} (n=1) s.c. xenografts two days after the last dose of the treatment period with MIR17PTi (on days 1-4-8-11), as compared to tumor retrieved from untreated animals (NCI-H929, n=1; AMO^{luc+}, n=1). Animals used for this analysis were not considered for tumor-growth and survival evaluations. The results shown are average pri-mir-17-92 expression levels after normalization with GAPDH and ΔΔCt calculations.

(**d**) qRT-PCR analysis (left panel) and western blotting (right panel) of BIM in retrieved tumors (AMO1) from MIR17PTi treated (n=1) or untreated (n=1) mice. The qRT-PCR results shown are average BIM expression levels after normalization with GAPDH and ΔΔCt calculations. GAPDH was used as protein loading control.

(**e**) Schematic representation of SCID-*hu* model (left panel) and INA-6 growth within human fetal bone chips s.c. implanted in NOD SCID mice (right panel). Plasmatic levels of soluble IL-6R were used to evaluate tumor growth. Systemic treatments with MIR17PTi (2mg/kg, days 1-4-8-15-22) started at day 22. Effects of MIR17PTi were evaluated at the end of treatments (day 44). A total of 8 mice was used as follows: NT (n=4), MIR17PTi (n=4).

**indicates p<0.05*

Fig. 7. Pharmacokinetics profile of MIR17PTi in *Cynomolgus* Monkeys

(**a**) Plasmatic PK profile (left panel) of MIR17PTi after injection of a Cynomolgus monkey with a single dose (0.504mg/kg). Sampling was performed at the time points indicated in the table (right panel).

(**b**) Plasmatic PK parameters of MIR17PTi in Cynomolgus monkeys.

Figure 1

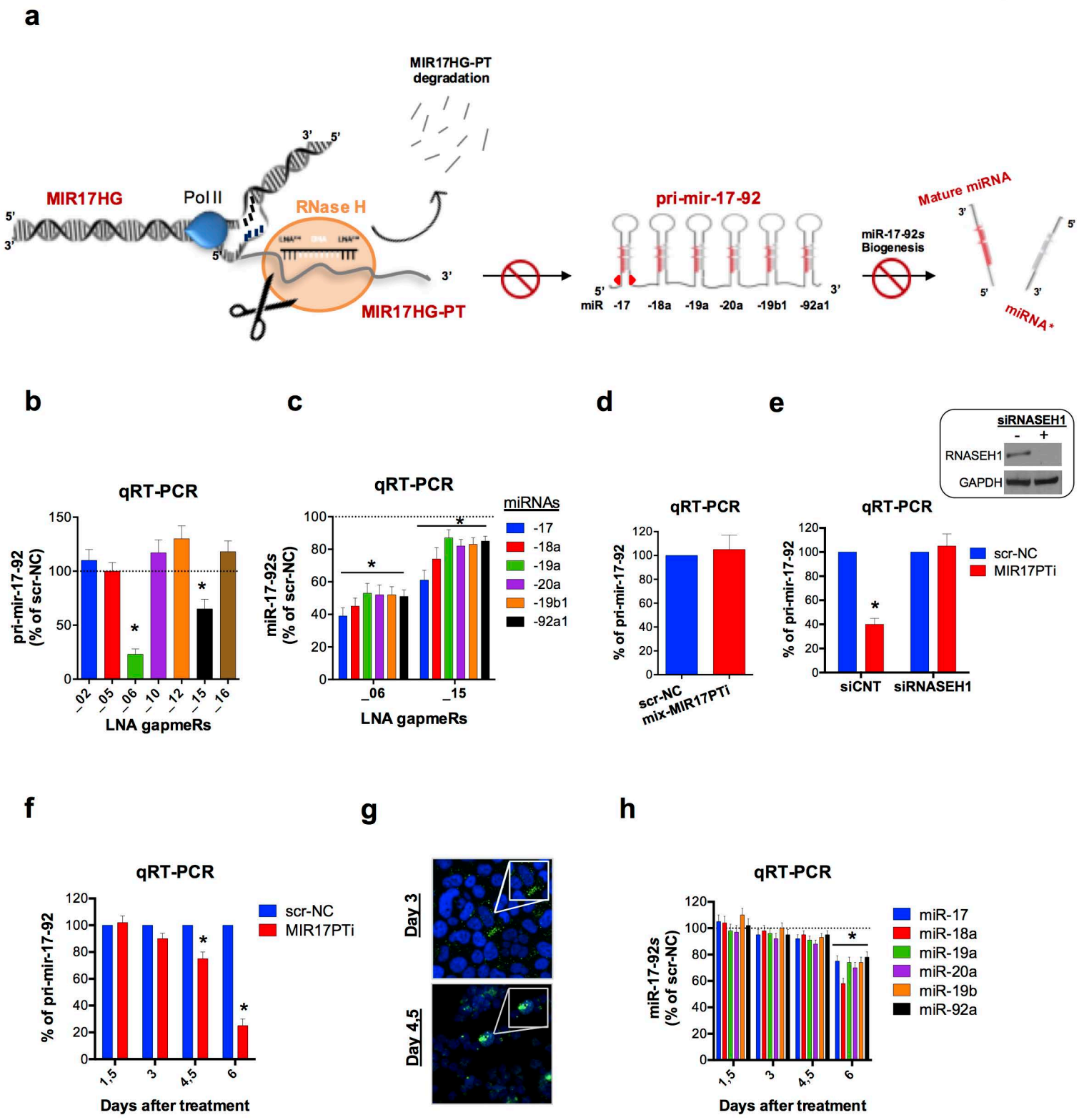

Figure 2

a

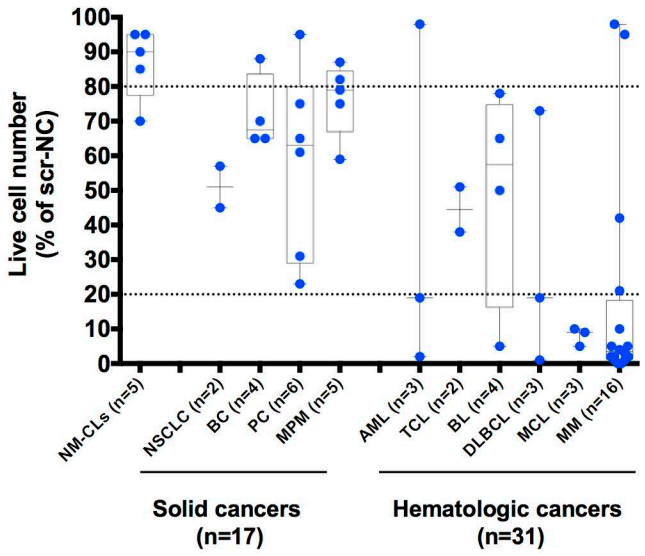

Insensitive: 293T, HK-2, HS-5, THLE-2 (NM-CLs); MCF-7 (BC); BxPC-3 (PC); Mero-14, MPM-376 (MPM); THP-1 (AML); SK-MM-1, OPM-2 (MM).

Moderately sensitive: HCC1143-BL (NM-CLs); LXF-289, A549 (NSCLC); MDA-231, HCC-1937 , SK-BR-3 (BC); Capan-1, Capan-2, ASPC-1, Panc-1, MiaPaca-2, (PC); MPM-209, IST-MES, Mero-25 (MPM); H9, Jurkat (TCL); P3HR1, Daudi, Raji (BL); Toledo (DLBCL); KMS-26 (MM).

Highly sensitive: K562, HL-60 (AML); Sultan (BL); Oci-Ly-7, Pfeiffer (DLBCL); Mino, Maver-1, Jeko-1 (MCL); AMO1, ABZB, ACFZ, MM.1S, MM.1R, NCI-H929, JJN3, KMS11, U266, LR7, KMS-12-BM, INA-6, RPMI-8226 (MM).

b

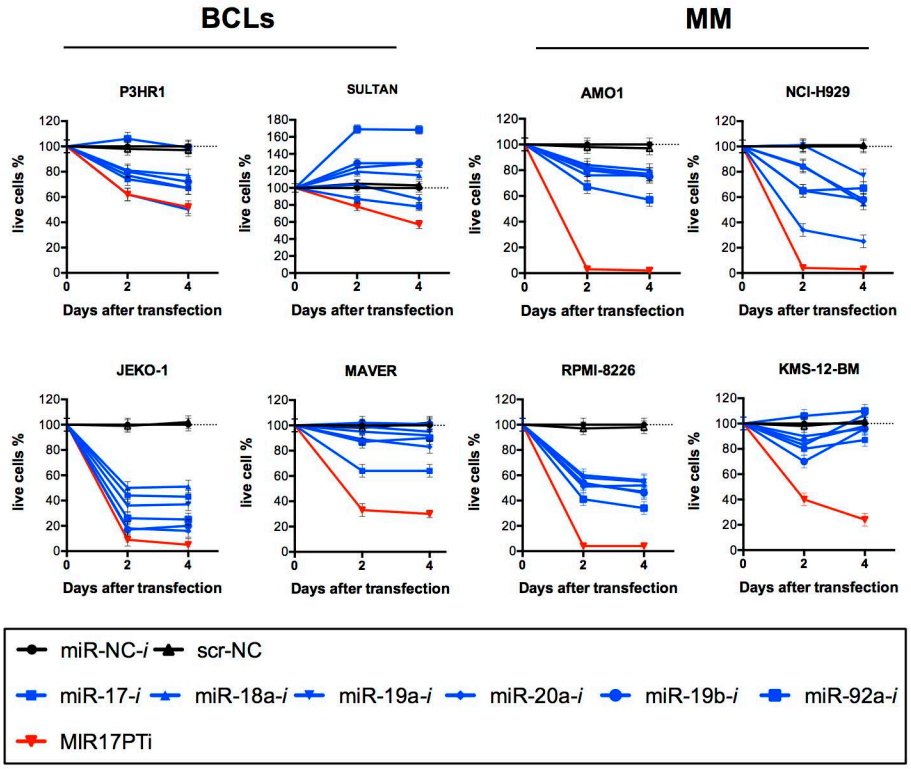

c

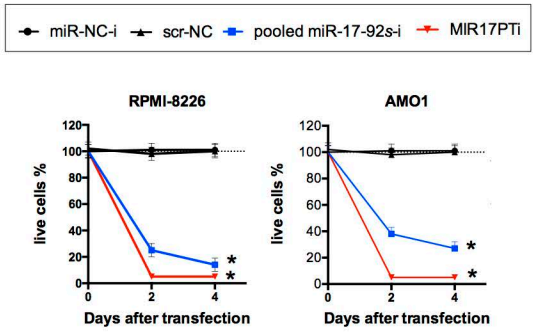

d

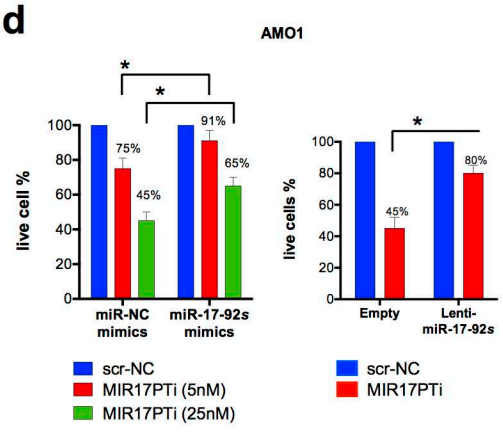

Figure 3

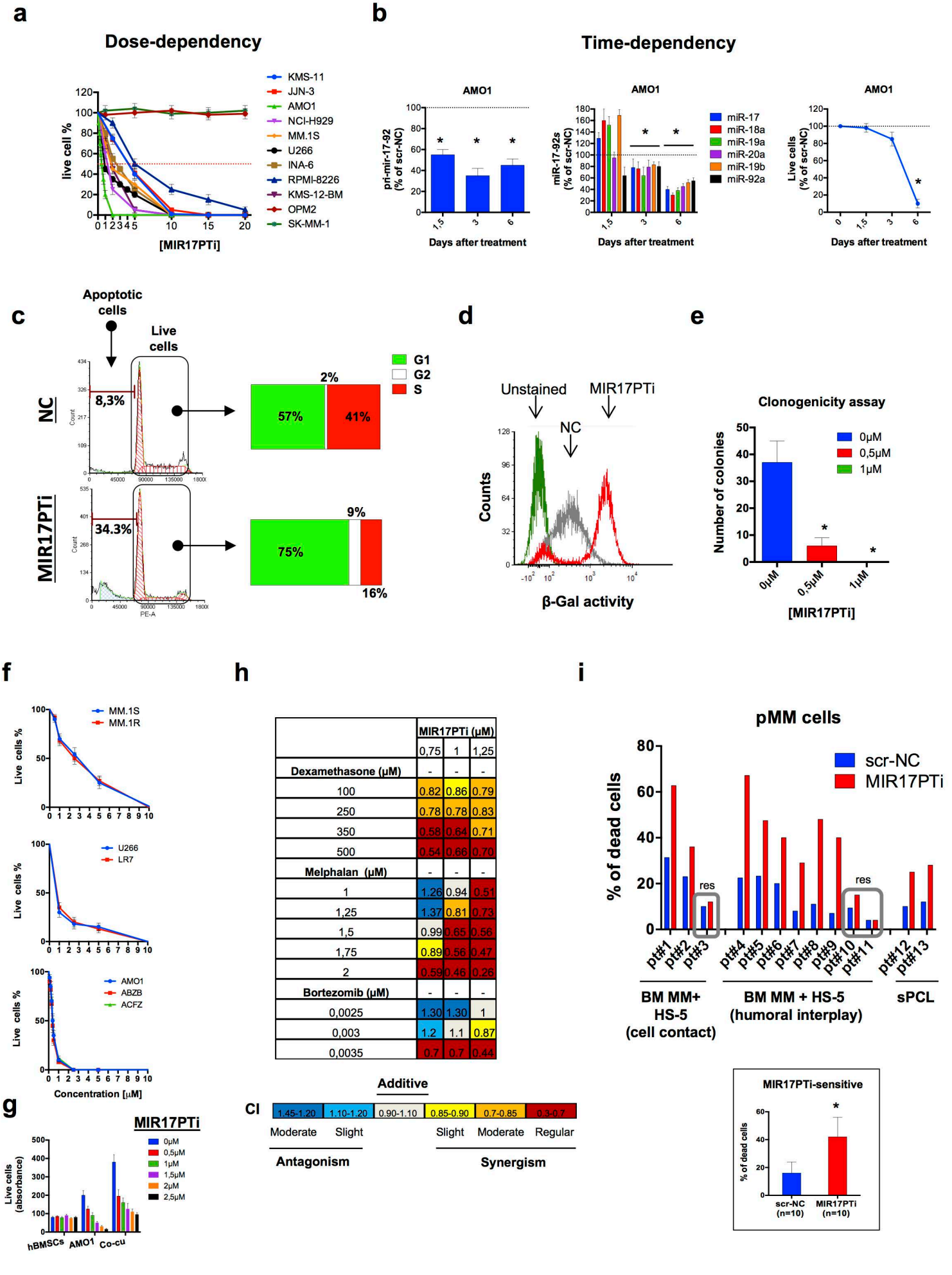

Figure 4

a

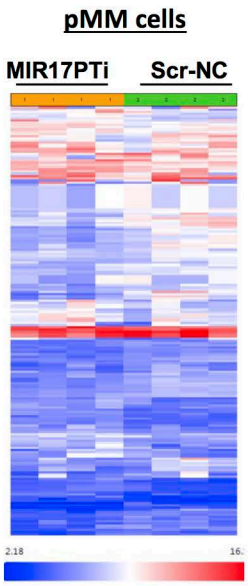

b

	Collection	Size	NES	FDR q-val
1	HALLMARK_MYC_TARGETS_V1	185	3,1	0.0
2	HALLMARK_TNFA_SIGNALING_VIA_NFKB	189	3,0	0.0
3	HALLMARK_G2M_CHECKPOINT	191	2,6	0.0
4	HALLMARK_APOPTOSIS	152	2,2	0.006
5	HALLMARK_OXIDATIVE_PHOSPHORYLATION	190	2,1	0.006
6	HALLMARK_MYC_TARGETS_V2	52	2,0	0.008
7	HALLMARK_INFLAMMATORY_RESPONSE	197	2,0	0.010
8	HALLMARK_P53_PATHWAY	192	1,8	0.034
9	HALLMARK_E2F_TARGETS	191	1,7	0.067
10	HALLMARK_WNT_BETA_CATENIN_SIGNALING	41	1,6	0.075

c

d

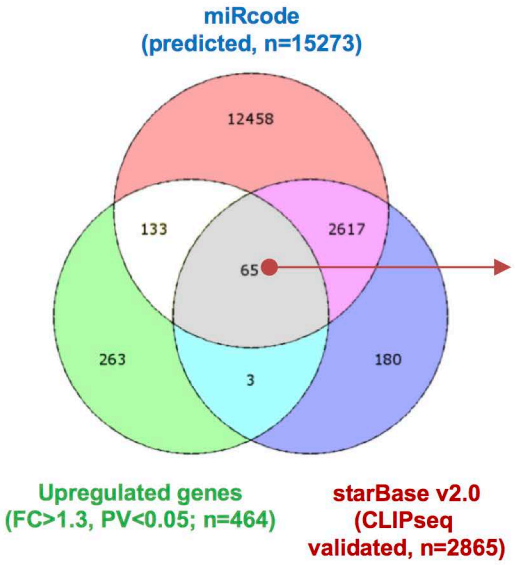

e

MYC /miR-17-92*s*
co-regulated
gene network
(n=15)

Incoherent FFLs:
- BCL2L11 (BIM)
- BICD2
- BZW2
- DUSP2
- IPO7
- MAT2A
- MLXIP
- NAP1L1
- SLC5A6
- VDAC1

Coherent FFLs:
- AKAP13
- GNAS
- PTK2B
- SKIL
- TRIM8

f

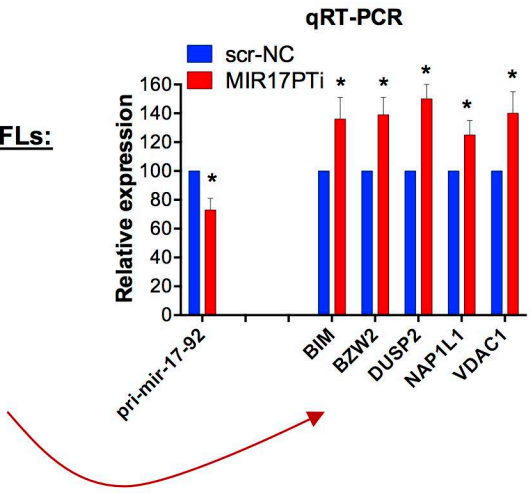

Figure 5

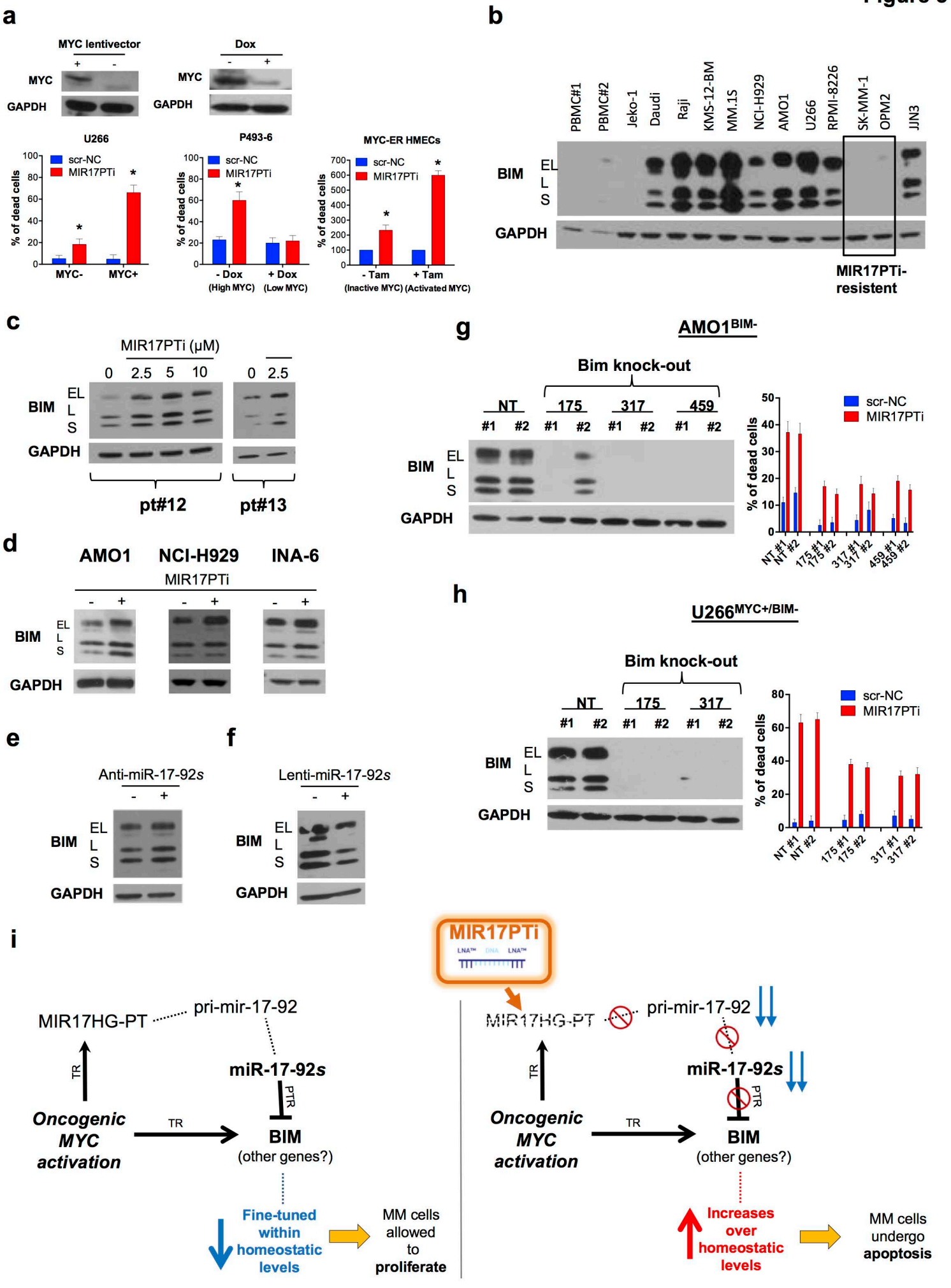

Figure 6

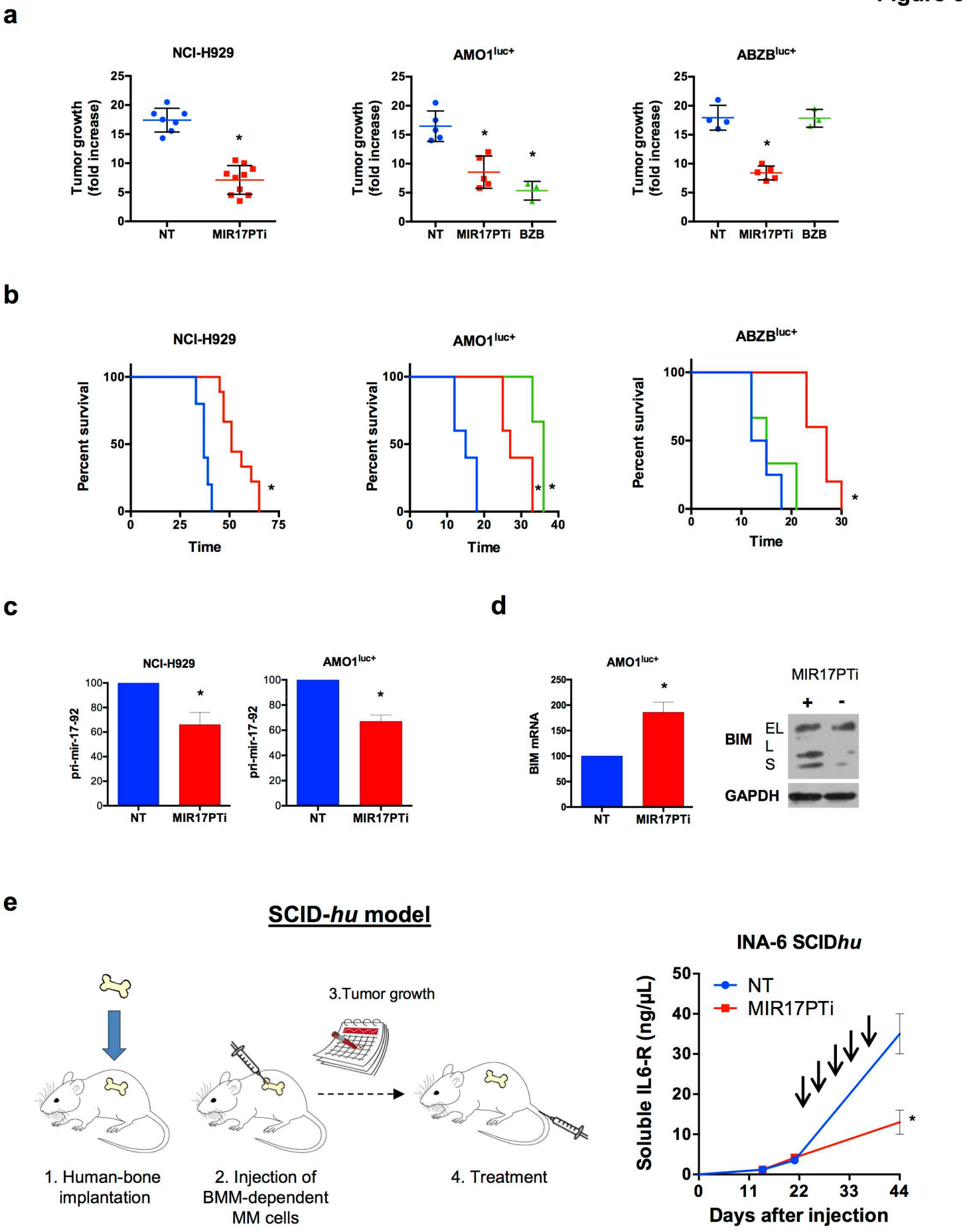

Figure 7

a

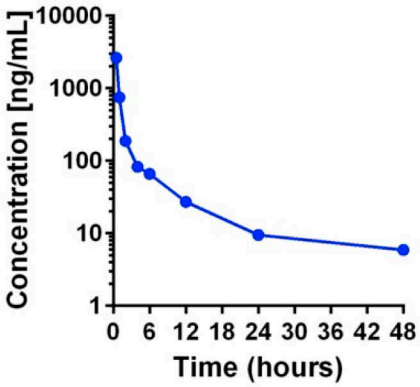

Time point (hours)	MIR17PTi (ng/mL)
Predose	0
0.5	2638
1	747
2	188
4	82
6	66
12	27
24	9
48	5

b

T_{max} (hr)	C_{max} (mg/mL)	AUC_{0-12} (hr * ng/mL)	$AUC_{0-\infty}$ (hr * ng/mL)
0.5	2,638	21,994	28,473

Prepublished online July 11, 2018;
doi:10.1182/blood-2018-03-836601 originally published online
July 11, 2018

Therapeutic vulnerability of multiple myeloma to MIR17PTi, a first-in-class inhibitor of pri-mir-17-92

Eugenio Morelli, Lavinia Biamonte, Cinzia Federico, Nicola Amodio, Maria Teresa Di Martino, Maria Eugenia Gallo Cantafio, Martina Manzoni, Francesca Scionti, Mehmet Kemal Samur, Annamaria Gullà, Maria Angelica Stamato, Maria Rita Pitari, Daniele Caracciolo, Settimio Sesti, Niels M. Frandsen, Marco Rossi, Antonino Neri, Mariateresa Fulciniti, Nikhil C. Munshi, Pierosandro Tagliaferri and Pierfrancesco Tassone

Blood (print ISSN 0006-4971, online ISSN 1528-0020), is published weekly by the American Society of Hematology, 2021 L St, NW, Suite 900, Washington DC 20036.